Activation/suppression balances in rat Superior Colliculus encode the visual continuity illusion

Rita Gil*, Ana Mafalda Valente*, Noam Shemesh†

Champalimaud Research, Champalimaud Centre for the Unknown, Lisbon PT

* First two authors contributed equally to this work.

One Sentence Summary: The rat superior colliculus plays a critical role in the visual continuity illusion.

Word Count: 4813

†Correspondence:

Dr. Noam Shemesh

Champalimaud Research, Champalimaud Centre for the Unknown

Av. Brasilia 1400-038, Lisbon, Portugal.

E-mail: noam.shemesh@neuro.fchampalimaud.org

Phone number: +351 210 480 000 ext. #4467.

Abstract

The continuity illusion occurs when visual stimuli are presented at a sufficiently high frequency, thereby triggering a shift from the static to the dynamic vision mode. This facilitates perception of continuous and moving objects, which is key for interactions with the surrounding environment. However, how the continuity illusion is encoded along the entire visual pathway remains poorly understood, with disparate Flicker Fusion Frequency (FFF) measured at the retinal, cortical, and behavioural levels. Here, we combine a behavioural paradigm, functional-MRI (fMRI), and electrophysiological validation for studying the mechanisms underlying the encoding of the continuity illusion effect in the rat. Our behavioural measurements reported a Flicker Fusion Frequency (FFF) of 18±2 Hz. Remarkably, whole-pathway fMRI revealed marked zero-crossings from positive to negative fMRI signal regimes at the FF in the superior colliculus (SC) – an important visual saliency detector – but not in higher cortical or thalamic visual areas. Our electrophysiological recordings in SC explained the sources of these observations as arising from strong neuronal suppression when the continuity illusion is achieved. Combined, our data suggests that activation and suppression balances in SC play a critical role in encoding the continuity illusion effect.

Introduction

The mammalian visual system[1–4] has evolved ingenious ways for recognizing and extracting visual features that enable object perception[5,6] and visual motion detection[7–10], both essential for interacting with the external environment. The encoding of spatial resolution features along the entire visual pathway is well characterised, with most brain structures exhibiting topographical mappings[11–15] that systematically represent the visual space. By contrast, how visual systems resolve luminance changes over time[16,17] has yet to be explained on a systems level, with most studies focusing mostly on the retina[18–20] and/or the visual cortex (VC)[21–23].

One critical temporal phenomenon for visual encoding is the *continuity illusion effect*: when photons impinge on the retina, the visual pathway can operate in static vision mode – whereby every flash is encoded as a separate event promoting attention and novelty perception – or can shift to the dynamic vision mode, where flashing stimuli is "fused" and perceived as a continuous steady light[16,24,25]. The Flicker Fusion Frequency (FFF) threshold defines when the dynamic vision mode is achieved. Retinal cyto-organization – closely related to activity patterns in animals – strongly affect measured FFF thresholds[19,26,27]. Diurnal fast-moving animals such as birds possess high visual temporal resolution which enables the detection and processing of fast-moving stimuli, such as prey, obstacles, as well as maintaining formation when flying in flocks[24]. The FFF threshold also plays important roles in prey-predator interactions, for example, in the camouflage of moving prey, or predator detection (a dynamically changing appearance can elicit a startle/fear response in predators, giving prey an advantage to escape)[28]. Systemic medical conditions such as hepatic encephalopathy or eye disorders such as multiple sclerosis, cataract, or glaucoma, can also strongly affect the FFF threshold and thus visual perception[16,24].

Interestingly, FFF thresholds derived from behaviour[21,24,29–33] and electrophysiological recordings (electroretinograms (ERGs)[18–20] or cortical evoked potentials (cVEPs)[21–23]) are disparate. For example, hens do not appear to behaviourally perceive flicker frequencies above 75-87 Hz[24,34], while their ERG responses remained in phase with the flickering light at frequencies beyond 100 Hz[19]. Similar trends were observed in mice, where ERGs found FFF thresholds of around 30 Hz[18] while behavioural reports derived thresholds around 14 Hz[35]. Strikingly, the FFF thresholds measured via electrophysiological recordings in the cortical end of the visual processing pathway disagree with both behaviour and ERGs, suggesting that the encoding of the behaviourally relevant FFF threshold occurs along the pathway, rather than in its retinal or cortical extremes.

Here, we surmise that complex integrative processes such as FFF thresholding encoding require a whole-network level understanding (**Figure 1A**). Thus, we combined behavioural measurements, functional MRI (fMRI), and electrophysiological recordings, to investigate where and how the rat brain's visual pathway encodes the FFF threshold. We find that the Superior Colliculus (SC) is a critical junction for flicker fusion, where boosting and suppression of neural activity drives the continuity illusion perception.

Results

Rats report a FFF threshold of 18± 2 Hz

We designed a simple psychophysics behavioural task to determine the FFF threshold in rats (**Figure 1B** and **1C)**. Rats were placed in a box with three ports and trained to associate one port to continuous or to flicker light (c.f. Methods for more details on the training). Trials were initiated by poking in the central port for a fixed duration of 200 ms. Then, an overhead LED was turned on and provided either continuous or flashing light at various frequencies (see Methods for more information). The animals had to wait for 1000 ms, whereupon a pure tone sound was played, indicating that animals could report on the perceived nature of the stimulus by poking in the side port they associated with flicker/continuous light. The overhead LED turned off when the animals left the central port. The percentage of reports to the flicker port is shown for the tested frequencies in **Figure 1C**. Notably, as the frequency increases, the percentage of reports to the flicker port decreases, indicating that the animal tends to choose the continuous light port for higher frequencies. As expected, the easiest frequencies for the animal to discriminate (1 and 2 Hz, and the true continuous light conditions) exhibit the highest and lowest percentages of reports. As the difficultly level for discriminating between individual flashes increases, the continuity illusion regime is achieved: for the FFF threshold calculation a sigmoid curve was fitted to the average animal response and the intercept at 0.5 (considered to be "chance level") was taken. The calculated FFF threshold was 18±2 Hz and the confidence interval was defined via a bootstrap method (c.f. Methods).

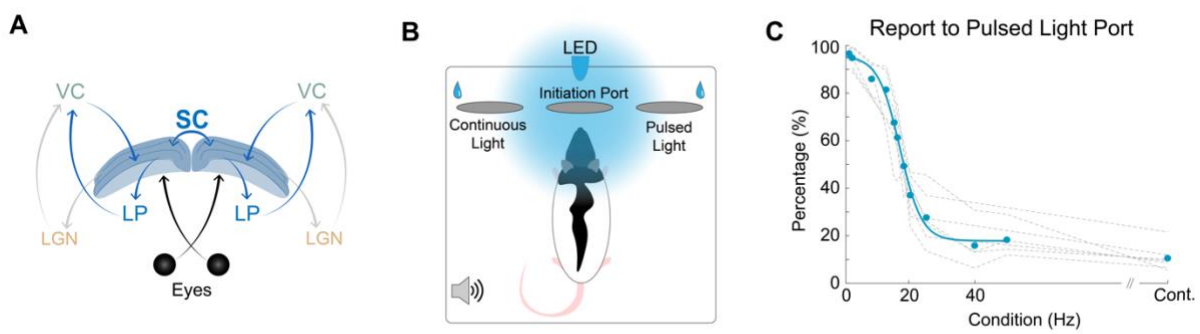

Figure 1. (A) Visual pathway schematic. The SC receives retinal inputs and projects to thalamic lateral geniculate (LGN) and lateroposterior (LP) nuclei. Information is passed to the visual cortex (VC) which sends corticotectal feedback projections back to SC. Tectotectal connections allow communication between the two SC's; **(B) Behaviour set-up schematic**. Water-deprived rats were placed in a dark box with three poking ports: a middle port to initiate trials and two lateral ports for continuous or flicker light reports. **(C) Percentage of reports to the pulsating port.** Thin grey dashed lines reflect the performance of each individual animal (N=7) while blue circles correspond to the averaged individual performances. As the frequency increases the animal reports less to the flickered port thus entering the continuity illusion regime. The calculated FFF threshold is 18±2 Hz.

Pathway-level fMRI reveals that SC signals tightly follow behavioural reports

We then turned to investigate activity in the entire visual pathway via functional-MRI (fMRI) experiments conducted at 9.4T with binocular simulation (spatial resolution of ~270×270 μm^2 in-plane, 1.5 mm slice thickness and 1.5 sec temporal resolution). The stimulation paradigm, and LED positioning,

relative to the animal's eyes, is shown in **Figure 2A**. Functional activation t-maps for representative stimulation frequencies of 1, 15, and 25 Hz are shown in **Figure 2B**. At the lowest stimulation frequency, strong positive Blood-Oxygenation-Level-Dependent (BOLD) responses (PBRs) are observed in subcortical structures of the visual pathway (SC and thalamic lateral geniculate nucleus of the thalamus – LGN). Cortical areas exhibit somewhat weaker PBRs. As the stimulation frequency increases, gradual shifts of PBRs to negative BOLD responses (NBRs) are observed first in VC and then in SC. LGN responses remained positive for all frequencies, but t-values decrease with frequency. ROI time-series (**Figure 2C**) confirmed the trends described above, and revealed sharp positive signals at the beginning and end of the higher frequency stimuli in SC (hereafter referred to as onset and offset signals, respectively) flanking a smaller "steady-state" fMRI response.

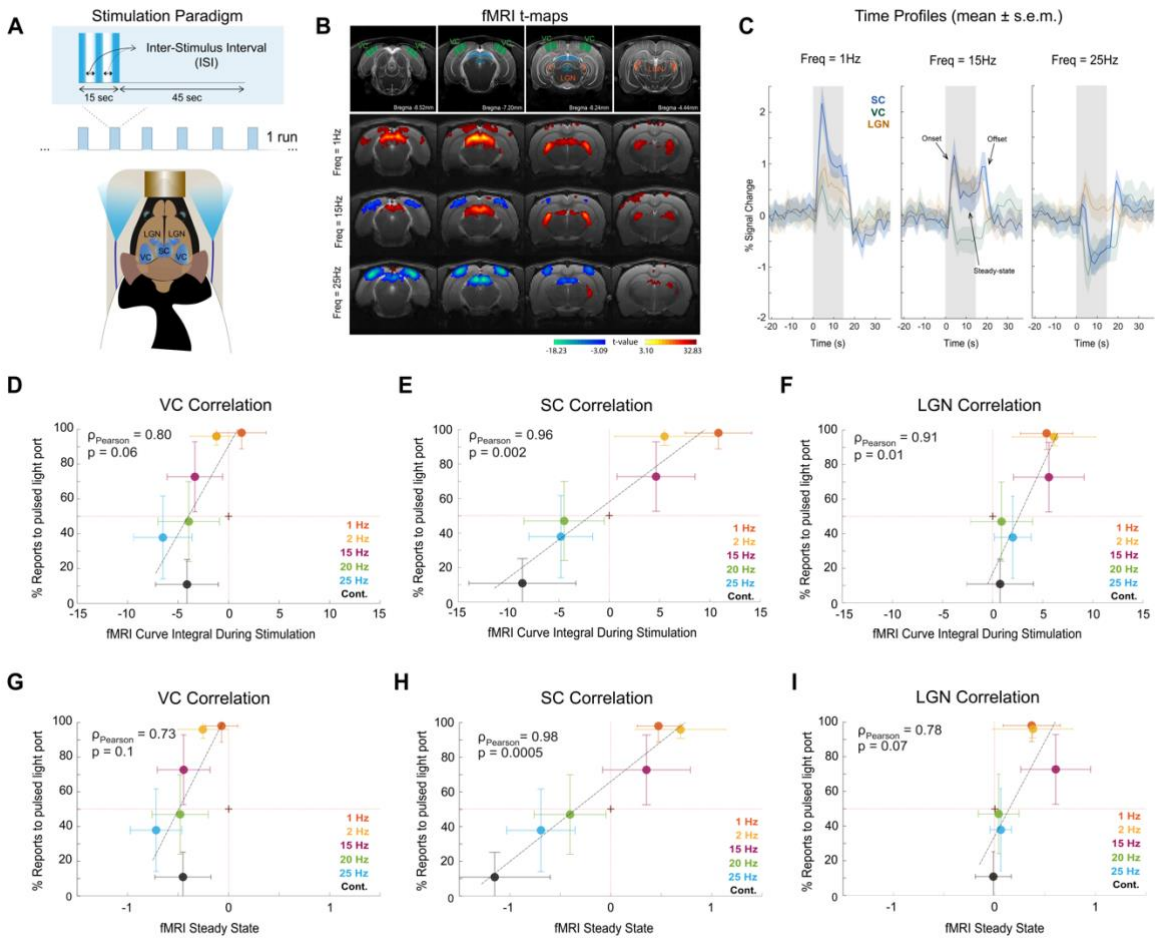

Figure 2: fMRI Results (A) TOP: Stimulation paradigm used in the fMRI and electrophysiology experiments. BOTTOM: Schematic of LEDs relative to the animal's eyes. (B) TOP: Anatomical MRI image with delineated ROIs and atlas overlapped. Different brain slices highlight visual pathway structures; **BOTTOM: fMRI t-maps for representative frequencies**. As the frequency of stimulation increases, transitions from PBRs to NBRs appear in VC and SC. **(C) fMRI signal time profiles.** Fine structure appears in fMRI responses. Onset and offset peaks, are evident in the SC profiles from 15 Hz onwards, along with a "steady-state" (all highlighted with black arrows on the 15 Hz plot); **Correlation of behaviour reports with (D-F) fMRI curve integral during stimulation and (G-I) "steady-state".** Coloured circles represent the average response of behavioural and fMRI sessions. Only the SC shows a clear transition from PBR to NBR that correlates with "chance level" reports.

To investigate how these fMRI responses correspond to FFF thresholds reported behaviourally by rats, we measured a larger stimulation frequency space in fMRI experiments. First, we correlated the fMRI curve integral during the entire stimulation period with behavioural reports (**Figures 2D, 2E** and **2F** for VC, SC and LGN, respectively). Strong correlations were observed for all three structures, with increasing fMRI responses associated with decreasing frequency. Interestingly, VC and LGN show saturated responses, i.e., for frequencies above 15 Hz, the negative VC responses remain rather constant and for LGN, above 20 Hz, the curves exhibit very small positive integral. Strikingly, SC exhibits a much broader dynamic range, and its fMRI signal integral crosses zero (i.e., a shift from PBR to NBR is observed) between 15-20 Hz, i.e., at the behaviourally measured FFF threshold. The PBR to NBR transition in SC closely tracks the shift of the animals' behavioural reports from flicker to continuous, suggesting that SC PBRs are associated with perception of pulsed lights, while NBRs reflect the continuity illusion effect at high stimulation frequencies.

To deconfound that the animals were exposed to the stimulus for only ~1 sec in the behavioural setting while in the fMRI experiments the stimulus exposure time was 15 sec, we analysed the fMRI curve at its "steady-state". **Figures 2G, 2H** and **2I** show the corresponding results. Notably, the SC exhibits the highest correlation coefficient of $\rho_{Pearson}$ = 0.98 (P=0.0005) while the VC and LGN show only moderate and statistically insignificant correlations of $\rho_{Pearson}$ = 0.73 (P=0.1) and $\rho_{Pearson}$ = 0.78 (P=0.07), respectively. Thus, the difference in stimulation duration between behaviour and fMRI is not a major confounding factor, as perhaps can be expected given that the animals choose whether a light is flickering or continuous on a fast timescale, but still perceive the flicker/continuous condition thereafter.

Electrophysiological recordings reveal that neuronal activation/suppression balances underpin PBR to NBR shifts in SC

As the SC showed the strongest behaviour-fMRI correlation, we targeted it for electrophysiological recordings (**Figure 3**). Fluorescence microscopy images (**Figure 3A**) validated the optimal angle of the silicon probe to record from the superficial layers of SC (SSC). **Figure 3B** and **3C** detail LFP traces (c.f **Figure S1** for zoomed in plots) and total spectral power over time between 1-50 Hz for the representative stimulation conditions, respectively (c.f. **Figure S2** for the rest of the conditions). Individual flashes clearly induce oscillations and strong power increases for the 1 Hz stimulation regime. At 15 Hz, much sharper power increases are observed at the edges of stimulation while more modest power increases can be seen during stimulation in the 15 Hz band (and some of its harmonics). By contrast, in the post-FFF threshold 25 Hz stimulation regime, oscillations are clearly absent during the stimulation period although the sharp onset and offset signals are still observed (**Figure 3B, 3C and S1)**.

To establish when "steady-state" signals are achieved for each stimulation condition, **Figures 3D, 3E and 3F** present the spectral power in the 1, 15 and 25 Hz frequency bins - highlighted with arrows in **Figure 3C**. Clearly, individual flash-induced power increases are present in the 1 Hz stimulation regime,

while a steady-state is reached after ~1-2 s of stimulation for 15 and 25 Hz, above and at baseline level, respectively. LFP and MUA time courses (**Figures 3G, 3H, 3I and 3J)** reveal the same characteristics, including onset, offset and steady-state signals.

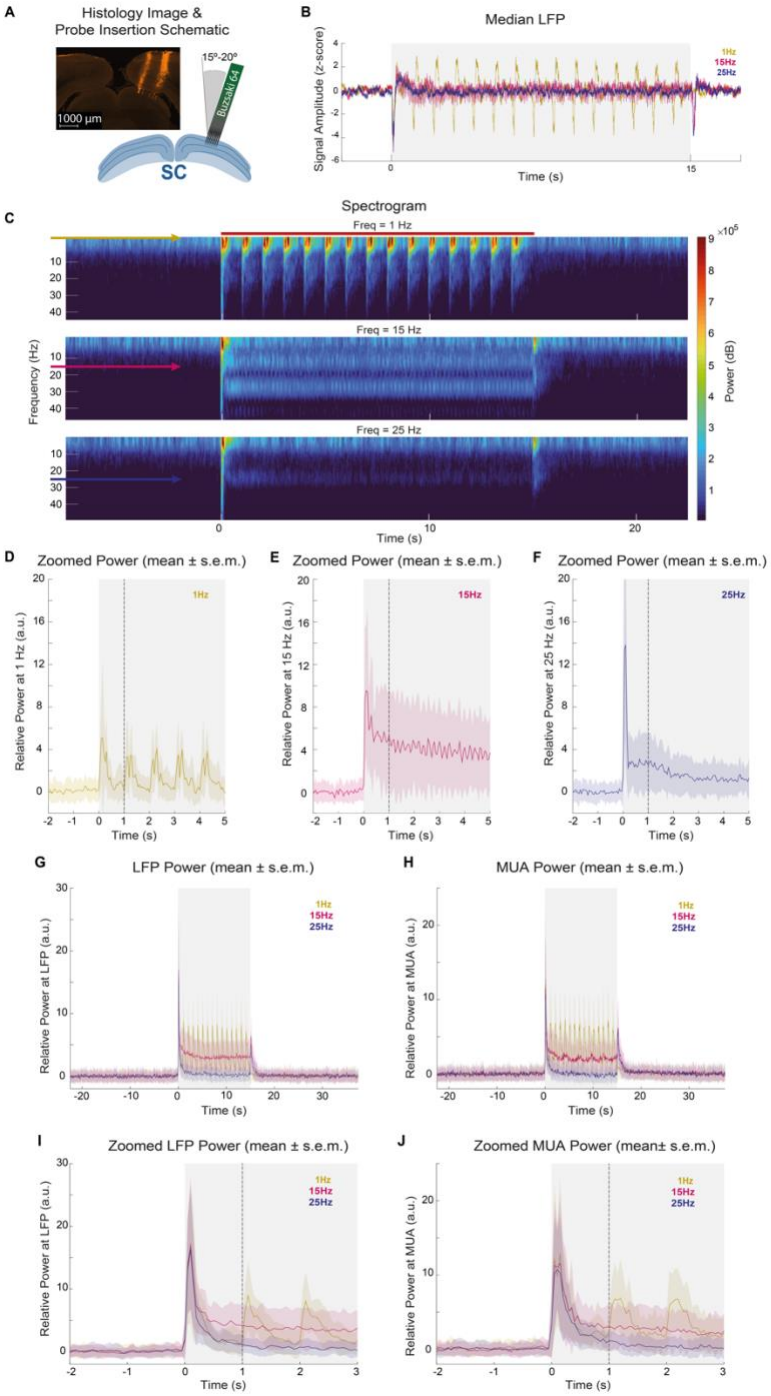

Figure 3: Electrophysiology Results. (A) Probe insertion schematic and fluorescence microscopy image; (B) Median LFP traces. LFP traces show individual flash-induced LFP oscillations for the 1 Hz condition but only onset and offset peaks for the higher frequencies; **(C) Spectrograms between 1-50 Hz for 1, 15 and 25 Hz stimulation regimes.** Arrows highlighting the 1, 15 and 25 Hz bins confirm trends observed; **(D-F) Power at the highlighted frequency bins.** A steady-state above and at baseline level is observed for 15 and 25 Hz stimulation, respectively, after 1 sec of stimulation. **(G and H) LFP and MUA relative power.** Both plots reveal a decreased power during stimulation as the frequency of stimulation increases. The steady-state observed at the two higher frequencies of stimulation is reached after 1 sec stimulation time, highlighted in **panels I and J.**

Activation / Suppression of neural activity underpins fMRI signal transitions in SC

To better explain the PBR to NBR transitions observed with fMRI in SC, we tested a broader range of visual stimulation frequencies both with fMRI and with electrophysiology. **Figures 4A and 4B** show the fMRI signals and MUA power in the SC, respectively. Together with our previous findings, these plots

support the premise that higher stimulation frequencies induce MUA power reductions – suppression of activity – that are evident as increasingly stronger NBRs. The fMRI-BOLD signals are naturally delayed compared with their fast MUA counterparts due to the complex neurovascular coupling mechanisms. Still, **Figure 4C** shows the 25 Hz MUA curve convolved with an HRF, which accurately approximates fMRI NBRs in SC - with onset and offset peaks appearing at similar time points as observed by fMRI. The same analysis is shown for LFPs **Figure S3** with similar results.

Figures 4D-I investigate the relationships between fMRI time-courses and their MUA counterparts both from a total integral perspective **(Figure 4D-F)** and at "steady-state" **(Figure 4G-I)** levels, the latter deconfounding onset/offset effects. At "steady-state", it becomes evident that stimuli below the FFF threshold induce fMRI and MUA positive signals, while stimuli above the FFF threshold lead to a strong reduction of fMRI and MUAs signals **(Figure 4G-I)**, again supporting a suppression of activity in SC when the continuity illusion is achieved. Note also the excellent, and statistically significant, correlations observed for both measurements (**Figure 4F and 4I)**. The lowest tested frequency (0.25 Hz) was excluded in **Figure 4F** and **4I** since at such low stimulation frequency, the four individual flashes represent four distinct stimuli never reaching "steady-state".

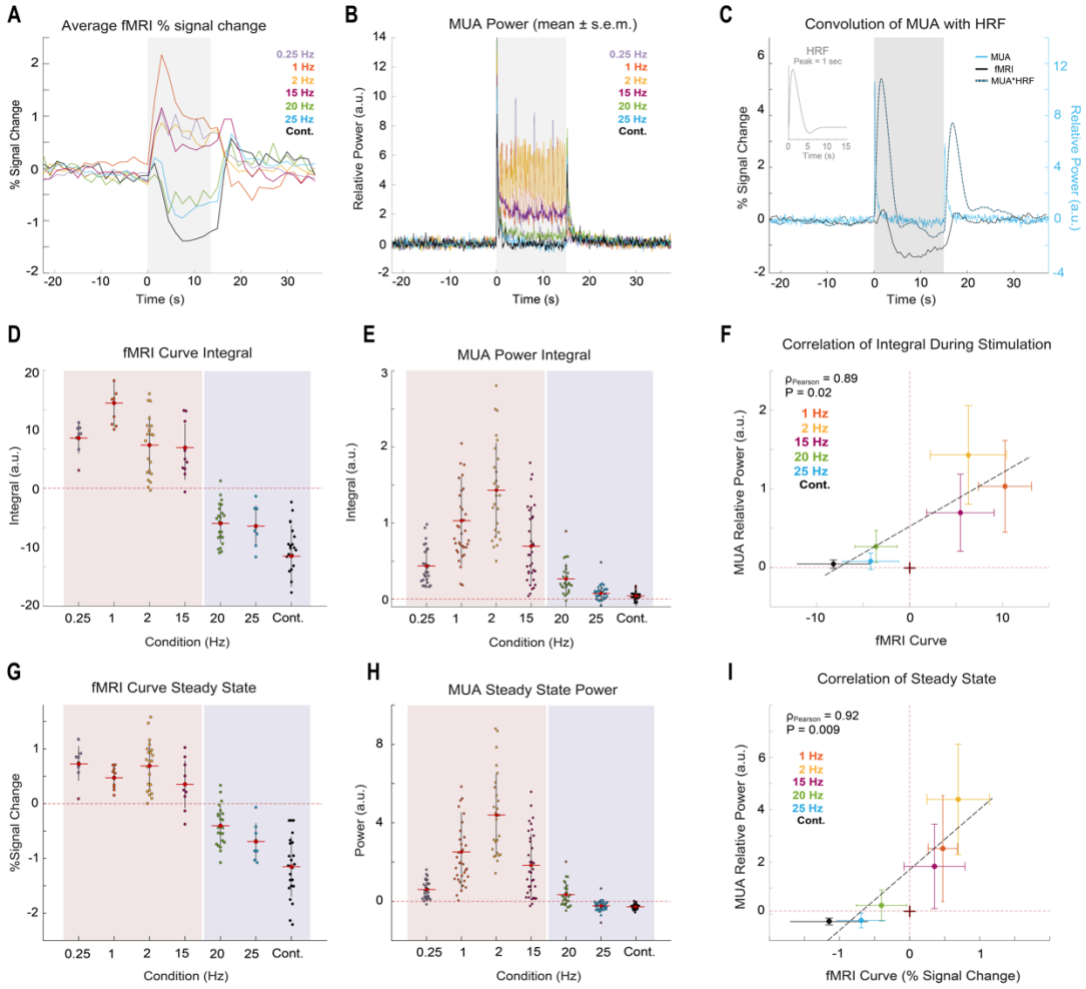

Figure 4: SC fMRI and MUA Correlation Results. (A) fMRI time profiles. Higher stimulation frequencies lead to stronger SC NBRs; **(B) MUA relative power.** Stronger power reduction is observed above the 20 Hz condition; **(C) Convolution of MUA with HRF peaking at 1 sec.** The resulting convolved MUA was compared with a fast fMRI acquisition (TR = 500 ms). Onset/offset peaks between the two curves are aligned with the first occurring 1.5-2sec after stimulation start and the latter appearing around 1.8-2.3 sec after stimulation ended;
(D) fMRI curve integral during stimulation. The first four frequencies show similar integral values while a clear reduction is observed at the NBR inducing frequencies. Frequencies presenting PBRs are shaded in light red while frequencies inducing NBRs are shaded in light blue; **(E) MUA power integral during stimulation.** An integral power increase is observed for the three lowest frequencies after which a reduction is clear from 15 Hz onwards; **(F) Correlation between MUA power and fMRI curve integral during stimulation.** A high correlation coefficient of $\rho_{Pearson}$ =0.89 (P=0.02) shows a tight relationship between the two measurements. NBRs at high stimulation frequencies correlate with strong MUA power reductions close to baseline levels; **(G) fMRI curve steady-state percent signal change.** Similar trend as seen in panel D; **(H) MUA power at steady-state.** Similar trend as seen in panel E; **(I) Correlation between steady-state MUA relative power and fMRI percent signal change.** A high correlation coefficient of $\rho_{Pearson}$=0.92 (P=0.009) similar to panel F confirms the close relationship between the two measurements.

Discussion

FFF thresholds are critical for visual perception. Studies focusing on the light entry point, the retina[18–20] in species that are more reliant on vision such as monkeys[29,41], dogs[31], cats[21,32,42,43] or birds[19,24,44], initially proposed that FFF thresholds rely solely on retinal function and rod/cone composition[22,36,37]. However, behaviourally-derived FFF thresholds were always lower than those derived from retinal electrophysiological recordings[19,24,34,35]. Hence, temporal resolution cannot be limited by the retina's ability to resolve flickers, but rather reflects processing that occurs along the visual pathway, where thresholds are likely modified at various stages[19,27]. Attempts to measure correlates of the visual continuity illusion at the perception level were carried out at the last neural information processing stage (VC)[21–23], where the lowest FFF threshold was reported in several species[36,38–40]. Thresholds for individual cells varied across a broad range of frequencies and importantly, the cortical FFF thresholds were lower than behaviourally-observed thresholds[22]. This underscores the importance of investigating FFF thresholds using a comprehensive experimental approach designed to directly measure behavioural FFF thresholds, and investigate activity correlates along the entire pathway.

Our behavioural results clearly revealed the continuity illusion phenomenon and provided the FFF threshold in rats (**Figure 1C)**. Since FFF thresholds may depend on task design[35], we focused on ensuring that our task would (i) avoid biasing the animals towards one side port; (ii) ensure that 50% of the trials would deliver continuous light; and (iii) limit presentation of frequencies above 8 Hz to only 10% of the flicker trials so that animals would not perceive the reward in the continuous stimulus as uncertain. The behavioural reports of an FFF threshold of 18±2 Hz are quite clear from **Figure 1C**, and further agrees with prior literature (~21 Hz in a different task[22,45]).

Our fMRI findings revealed that SC signals have the largest dynamic range of responses. Interestingly, their dependence of stimulation frequency bears the closest relationship with the continuity illusion as reported by behaviour: below the behaviourally measured FFF threshold, PBRs indicated an activation of the SC, while above the FFF threshold, NBRs were observed during the bulk of the stimulation period (aside from the onset/offset signals, vide-infra). When the continuity illusion is reached at even higher frequencies, the NBRs intensify in SC. A plausible mechanistic hypothesis for these signals in SC would suggest activation upon perceiving flickering light (PBRs) and suppression of neural activity (NBRs) above the FFF threshold and when reaching the continuity illusion. Our electrophysiological findings in SC – targeted due to the clear fMRI responses – further lent credence to this hypothesis by evidencing decreases in power to baseline levels at high stimulation frequencies and strong transients at lower frequencies. Taken together, the fMRI and electrophysiological findings suggest that activation/suppression balances in the SC are potential drivers of the perceived continuity illusion effect.

Anatomically two visual sub-pathways co-exist: the extrageniculate (including SC) and the geniculate (including LGN) pathways. Experiments[21,46] lesioning either one or the other revealed different roles in FFF threshold determination: while the geniculate pathway mediates high flicker frequencies, the extrageniculate pathway mediates lower frequencies. The SC would behave as a lowpass filter limiting high frequency perception, in line with our findings that the SC plays an active role for the FFF threshold

determination. Experiments looking into the involvement of the VC in flicker discrimination revealed that, while humans became insensitive to any form of light stimulation following cortical ablation, lower-order species such as cats[47] and albino rats[38], remained able to discriminate flicker from steady light. This suggests subcortical "fusion mechanisms" in lower-order species.

In the context of continuity illusion, few studies investigated SC[21,46]; rather, SC has been widely studied in the context of response habituation[48,49] (RH), a phenomenon which, similarly to the continuity illusion effect, occurs in the SSC at high stimulation frequencies. RH is expected to serve as a form of short-term memory for familiar versus novel information based on the dynamic adjustment of response thresholds. Studies[49–52] have suggested a mechanism of feedback inhibition to be behind RH: the co-activation of excitatory and inhibitory neurons leads to a long-lasting inhibition blocking responses to subsequent stimulus presentation at high enough frequencies. The RH effect may be a contributor to the continuity illusion effect (probably among other mechanisms occurring long the visual pathway) and, if indeed the two phenomena are related, the continuity illusion effect in the SC would result, in part, from inhibitory processes - in line with the measured neuronal suppression at high stimulation frequencies both via fMRI and MUAs.

Another interesting finding in this study, is the ability of BOLD-fMRI to resolve the onset/offset peaks at the high frequency stimulation regimes. Onset peaks have previously been described in the SC[53–55] - at different stimulation frequencies, responses to the first flash remained similar and only subsequent responses appeared reduced in amplitude. However, to our knowledge, this is the first time in which offset peaks have been described in the SC at high frequency regimes. Co-activation of excitatory and inhibitory neurons[52] alone is unlikely to fully explain the observed offset signals, suggesting that the measured neuronal suppression occurring during the stimulation period might be an active process, and not solely the result of different and lasting simultaneous effects. One interpretation could be that when individual flashes are no longer perceptible, the entire stimulation period is integrated as "one long flash" and the SC onset/offset peaks reflect brightness changes detected at the edges of stimulation – from dark to bright (onset peak) and from bright to dark (offset peak).

Finally, it is worth mentioning that our work provides insight into the ongoing debate on the nature of negative BOLD signals and their underlying biological underpinnings. The correlations between MUA and NBRs in this study point to neuronal supression[56–65] as the most probable scenario, and provide a system where the amplitude of the NBR can be modulated by a simple experimental variable – the stimulation frequency – which could serve as an experimental handle for future research into the mechanisms underlying the NBR neurovascular coupling.

Several limitations can be noted for this study. First, animals are awake during the behavioural task, while they are kept under light sedation (medetomidine, an alpha-2-adrenoreceptor agonist commonly used in fMRI studies) during fMRI and electrophysiology data acquisition, which could potentially confound perceptual behavioural reports and neural/BOLD signals. Still the good agreement between the measurements suggests that this would not be a critical effect here. Second, we note that the percentage of reports to the flicker port (**Figure 1C**), in the continuous light condition does not correspond to 0% flicker reports, and we consider that this level of performance does not reflect true lapses nor a limitation of the

used LEDs, but rather a limitation of the task itself. Presenting probe trials in 10% of the flicker trials may have been sufficient for the animals to perceive reward for the continuous light stimulus as uncertain thus lower their performance (see supplementary discussion in **Figure S5**). Perhaps, repeating the same task with a lower percentage of probe trials or changing the reward systems for these would reduce this issue. Third, the animals made their behavioural reports after 1 sec of stimulus presentation, while in the fMRI and electrophysiological sessions, stimuli lasted for 15 sec. This prompted the analyses shown in **Figure 3I and 3J**, where we show that at this time neural signals already reached a steady-state, observed in fMRI with the time lag due to the neurovascular couplings' dynamics. Furthermore, the excellent tracking of fMRI signals from MUA is depicted in **Figure 4C** where the NBR at the 25 Hz can be fully predicted from the MUA curve convolution with a conventional HRF. This is a good indicator that "steady-state" fMRI signal can be used with good confidence as a proxy for the MUA recordings and consequently, also explain the behavioural reports.

Conclusions

The continuity illusion phenomenon was investigated in the rat through behaviour, fMRI and electrophysiological recordings. We find a strong agreement between behaviourally measured FFF thresholds and zero crossings of SC fMRI signals, which suggests that this structure is dominant for continuity illusion effect encoding through activation and suppression of activity below and above the FFF threshold. This is supported by SC's location and functional connections within the visual pathway and its role in visual saliency detection. Importantly, we provide a direct behavioural interpretation for the measured SC NBRs at high stimulation frequency regime. Finally, the excellent agreement between electrophysiology and fMRI measurements lends further credence to SC's role in the continuity illusion effect.

Acknowledgments

The authors would like to thank Dr. Cristina Chavarrías for the implementation of the fMRI in the acquisition MRI sequences and Ms. Francisca Fernandes for the fMRI analysis MATLAB code which was used for the generation of the BOLD t-maps. The authors would also like to thank Dr. Bruno Cruz, Dr. Tiago Monteiro, and Mr. Filipe Rodrigues for the input regarding the behaviour experimental design. Finally, the authors would like to especially thank Mr. Juan Castiñeiras and Mr. Tiago Costa for advice on data analysis.

References

1. Nassi, J. J. & Callaway, E. M. Parallel processing strategies of the primate visual system. *Nat. Rev. Neurosci.* **10**, 360–372 (2009).
2. Schlag, J. & Schlag-Rey, M. Through the eye, slowly; Delays and localization errors in the visual system. *Nat. Rev. Neurosci.* **3**, 191–200 (2002).
3. Siegle, J. H. *et al.* Survey of spiking in the mouse visual system reveals functional hierarchy. *Nature* **592**, 86–92 (2021).
4. Sabesan, R., Schmidt, B. P., Tuten, W. S. & Roorda, A. The elementary representation of spatial and color vision in the human retina. *Sci. Adv.* **2**, (2016).
5. Basso, M. A., Bickford, M. E. & Cang, J. Unraveling circuits of visual perception and cognition through the superior colliculus. *Neuron* **109**, 918–937 (2021).
6. White, B. J. *et al.* Superior colliculus neurons encode a visual saliency map during free viewing of natural dynamic video. *Nat. Commun.* **8**, 2–10 (2017).
7. Ge, X. *et al.* Retinal waves prime visual motion detection by simulating future optic flow. *Science (80-.).* **373**, (2021).
8. Li, Y. tang, Turan, Z. & Meister, M. Functional Architecture of Motion Direction in the Mouse Superior Colliculus. *Curr. Biol.* **30**, 3304-3315.e4 (2020).
9. de Malmazet, D., Kühn, N. K. & Farrow, K. Retinotopic Separation of Nasal and Temporal Motion Selectivity in the Mouse Superior Colliculus. *Curr. Biol.* **28**, 2961-2969.e4 (2018).
10. Beltramo, R. & Scanziani, M. A collicular visual cortex: Neocortical space for an ancient midbrain visual structure. *Science (80-.).* **363**, 64–69 (2019).
11. Reber, M., Burrola, P. & Lemke, G. A relative signalling model for the formation of a topographic neural map. *Nature* **431**, 847–853 (2004).
12. Feinberg, E. H. & Meister, M. Orientation columns in the mouse superior colliculus. *Nature* **519**, 229–232 (2015).
13. Hafed, Z. M. & Chen, C. Y. Sharper, Stronger, Faster Upper Visual Field Representation in Primate Superior Colliculus. *Curr. Biol.* **26**, 1647–1658 (2016).
14. Seabrook, T. A., Burbridge, T. J., Crair, M. C. & Huberman, A. D. Architecture, Function, and Assembly of the Mouse Visual System. *Annual Review of Neuroscience* **40**, 499–538 (2017).
15. Arcaro, M. J., Honey, C. J., Mruczek, R. E. B., Kastner, S. & Hasson, U. Widespread correlation patterns of fMRI signal across visual cortex reflect eccentricity organization. *Elife* **2015**, 1–28 (2015).
16. Eisen-Enosh, A., Farah, N., Burgansky-Eliash, Z., Polat, U. & Mandel, Y. Evaluation of Critical Flicker-Fusion Frequency Measurement Methods for the Investigation of Visual Temporal Resolution. *Sci. Rep.* **7**, 2–10 (2017).
17. Boström, J. E. *et al.* Ultra-Rapid vision in birds. *PLoS One* **11**, 3–9 (2016).
18. Yang, S. *et al.* The electroretinogram of mongolian gerbil (Meriones unguiculatus): Comparison to mouse. *Neurosci. Lett.* **589**, 7–12 (2015).
19. Lisney, T. J., Ekesten, B., Tauson, R., Håstad, O. & Ödeen, A. Using electroretinograms to assess flicker fusion frequency in domestic hens Gallus gallus domesticus. *Vision Res.* **62**, 125–133 (2012).
20. Gilmour, G. S. *et al.* The electroretinogram (ERG) of a diurnal cone-rich laboratory rodent, the Nile grass rat (Arvicanthis niloticus). *Vision Res.* **48**, 2723–2731 (2008).
21. Schwartz, A. S. Electrophysiological correlates of flicker perception in the cat. *Physiol. Behav.* **8**, 603–609 (1972).
22. Wells, E. F., Bernstein, G. M., Scott, B. W., Bennett, P. J. & Mendelson, J. R. Critical flicker frequency responses in visual cortex. *Exp. Brain Res.* **139**, 106–110 (2001).
23. Schneider, C. W. Electrophysiological analysis of the mechanisms underlying critical flicker frequency. *Vision Res.* **8**, 1235–1244 (1968).
24. Lisney, T. J. *et al.* Behavioural assessment of flicker fusion frequency in chicken Gallus gallus domesticus. *Vision Res.* **51**, 1324–1332 (2011).

25. Mankowska, N. D. *et al.* Critical flicker fusion frequency: A narrative review. *Med.* **57**, 1–9 (2021).
26. Landis, C. Determinants of the critical flicker-fusion threshold. *Physiol. Rev.* **34**, 259–286 (1954).
27. Euler, T. & Wässle, H. Immunocytochemical identification of cone bipolar cells in the rat retina. *J. Comp. Neurol.* **361**, 461–478 (1995).
28. Umeton, D., Read, J. C. A. & Rowe, C. Unravelling the illusion of flicker fusion. *Biol. Lett.* **13**, (2017).
29. Shumake, S. A., Smith, J. C. & Taylor, H. L. Critical Fusion Frequency in Rhesus Monkeys. *Psychol. Rec.* **18**, 537–542 (1968).
30. Anderson, K. V. & Keith O'Steen, W. Altered response latencies on visual discrimination tasks in rats with damaged retinas. *Physiol. Behav.* **12**, 633–637 (1974).
31. Coile, D. C., Pollitz, C. H. & Smith, J. C. Behavioral determination of critical flicker fusion in dogs. *Physiol. Behav.* **45**, 1087–1092 (1989).
32. Schwartz, A. S. & Cheney, C. Neural mechanisms involved in the critical flicker frequency of the cat. **1**, 369–380 (1966).
33. Hendricks, J. Flicker Thresholds as Determined by a Modified Conditioned Suppression Procedure. *J. Exp. Anal. Behav.* **9**, (1966).
34. Rubene, D., Håstad, O., Tauson, R., Wall, H. & Ödeen, A. The presence of UV wavelengths improves the temporal resolution of the avian visual system. *J. Exp. Biol.* **213**, 3357–3363 (2010).
35. Nomura, Y. *et al.* Evaluation of critical flicker-fusion frequency measurement methods using a touchscreen-based visual temporal discrimination task in the behaving mouse. *Neurosci. Res.* **148**, 28–33 (2019).
36. Brozek, E. S. and J. Flicker Fusion Frequency Background and Applications. *J. Physiol.* (1952).
37. Van de Grind, W. A., Grusser, O. J. & Lunkenheimer, H. U. Temporal transfer properties of the afferent visual system. *Handb. Sens. Physiol. Cent. Vis. Information, A* 431–573 (1973).
38. Schwartz, A. S. & Clark, G. Discrimination of intermittent photic stimulation in the rat without its striate cortex. *J. Comp. Physiol. Psychol.* **50**, 468–471 (1957).
39. Grubb, M. S. & Thompson, I. D. Quantitative Characterization of Visual Response Properties in the Mouse Dorsal Lateral Geniculate Nucleus. *J. Neurophysiol.* **90**, 3594–3607 (2003).
40. Hawken, M. J., Shapley, R. M. & Grosof, D. H. Temporal-frequency selectivity in monkey visual cortex. *Vis. Neurosci.* **13**, 477–492 (1996).

Figure captions

Figure 1. (A) Visual pathway schematic. The SC receives retinal inputs and projects to thalamic lateral geniculate (LGN) and lateroposterior (LP) nuclei. Information is passed to the visual cortex (VC) which sends corticotectal feedback projections back to SC. Tectotectal connections allow communication between the two SC's; **(B) Behaviour set-up schematic**. Water-deprived rats were placed in a dark box with three poking ports: a middle port to initiate trials and two lateral ports for continuous or flicker light reports. **(C) Percentage of reports to the pulsating port.** Thin grey dashed lines reflect the performance of each individual animal (N=7) while blue circles correspond to the averaged individual performances. As the frequency increases the animal reports less to the flickered port thus entering the continuity illusion regime. The calculated FFF threshold is 18±2 Hz.

Figure 2: fMRI Results (A) TOP: Stimulation paradigm used in the fMRI and electrophysiology experiments. BOTTOM: Schematic of LEDs relative to the animal's eyes. (B) TOP: Anatomical MRI image with delineated ROIs and atlas overlapped. Different brain slices highlight visual pathway structures; **BOTTOM: fMRI t-maps for representative frequencies**. As the frequency of stimulation increases, transitions from PBRs to NBRs appear in VC and SC. **(C) fMRI signal time profiles.** Fine structure appears in fMRI responses. Onset and offset peaks, are evident in the SC profiles from 15 Hz onwards, along with a "steady-state" (all highlighted with black arrows on the 15 Hz plot); **Correlation of behaviour reports with (D-F) fMRI curve integral during stimulation and (G-I) "steady-state".** Coloured circles represent the average response of behavioural and fMRI sessions. Only the SC shows a clear transition from PBR to NBR that correlates with "chance level" reports.

Figure 3: Electrophysiology Results. (A) Probe insertion schematic and fluorescence microscopy image; (B) Median LFP traces. LFP traces show individual flash-induced LFP oscillations for the 1 Hz condition but only onset and offset peaks for the higher frequencies; **(C) Spectrograms between 1-50 Hz for 1, 15 and 25 Hz stimulation regimes.** Arrows highlighting the 1, 15 and 25 Hz bins confirm trends observed; **(D-F) Power at the highlighted frequency bins.** A steady-state above and at baseline level is observed for 15 and 25 Hz stimulation, respectively, after 1 sec of stimulation. **(G and H) LFP and MUA relative power.** Both plots reveal a decreased power during stimulation as the frequency of stimulation increases. The steady-state observed at the two higher frequencies of stimulation is reached after 1 sec stimulation time, highlighted in **panels I and J.**

Figure 4: SC fMRI and MUA Correlation Results. (A) fMRI time profiles. Higher stimulation frequencies lead to stronger SC NBRs; **(B) MUA relative power.** Stronger power reduction is observed above the 20 Hz condition; **(C) Convolution of MUA with HRF peaking at 1 sec.** The resulting convolved MUA was compared with a fast fMRI acquisition (TR = 500 ms). Onset/offset peaks between the two curves are aligned with the first occurring 1.5-2sec after stimulation start and the latter appearing around 1.8-2.3 sec after stimulation ended;
(D) fMRI curve integral during stimulation. The first four frequencies show similar integral values while a clear reduction is observed at the NBR inducing frequencies. Frequencies presenting PBRs are shaded in light red while frequencies inducing NBRs are shaded in light blue; **(E) MUA power integral during stimulation.** An integral power increase is observed for the three lowest frequencies after which a reduction is clear from 15 Hz onwards; **(F) Correlation between MUA power and fMRI curve integral during stimulation.** A high correlation coefficient of $\rho_{Pearson}$ =0.89 (P=0.02) shows a tight relationship between the two measurements. NBRs at high stimulation frequencies correlate with strong MUA power reductions close to baseline levels; **(G) fMRI curve steady-state percent signal change.** Similar trend as seen in panel D; **(H) MUA power at steady-state.** Similar trend as seen in panel E; **(I) Correlation between steady-state**

MUA relative power and fMRI percent signal change. A high correlation coefficient of $\rho_{Pearson}$=0.92 (P=0.009) similar to panel F confirms the close relationship between the two measurements.